JOURNAL OF GEOPHYSICAL RESEARCH, VOL. 113, A08105, doi:10.1029/2007JA012711, 2008

Turbulence transport throughout the heliosphere

B. Breech,[1] W. H. Matthaeus,[1] J. Minnie,[1] J. W. Bieber,[1] S. Oughton,[2] C. W. Smith,[3] and P. A. Isenberg[3]

Received 3 August 2007; revised 20 November 2007; accepted 13 March 2008; published 7 August 2008.

[1] We employ a turbulence transport model to compute distributions of turbulence throughout the heliosphere. The model determines the radial dependence of three (coupled) quantities that characterize interplanetary turbulence, the energy per unit mass, the cross helicity or Alfvénicity, and a similarity length scale. A fourth integrated quantity, the plasma temperature, is modified by heat deposition due to turbulent dissipation. The model includes advection, expansion, and reflection effects as well as the tendency toward dynamic alignment, and a von Kármán type dissipation function that represents decay of turbulence due to cascade to small scales. Two types of forcing are also featured, one a simple model of stream shear, and the other a driving in the outer heliosphere associated with wave energy injection due to pickup protons of interstellar origin. Parameters for the model have been tuned using observation data from Voyager and Ulysses. We analyze the constraining observations to provide boundary conditions and parameters that vary with heliocentric latitude, with some extrapolations. The fully assembled model permits the computation of the distribution of turbulence throughout the entire heliosphere, and we present solutions for several appropriate parameter sets.

Citation: Breech, B., W. H. Matthaeus, J. Minnie, J. W. Bieber, S. Oughton, C. W. Smith, and P. A. Isenberg (2008), Turbulence transport throughout the heliosphere, *J. Geophys. Res.*, *113*, A08105, doi:10.1029/2007JA012711.

1. Introduction

[2] It is now well established that the radial evolution of interplanetary hydromagnetic turbulence in the heliosphere is not fully accounted for by theories based on noninteracting waves, such as WKB theory [e.g., *Bavassano et al.*, 1982a, 1982b; *Roberts et al.*, 1987a, 1987b; *Matthaeus et al.*, 1990; *Smith et al.*, 2001; *Oughton*, 2003; *Bruno and Carbone*, 2005]. Here we refer to fluctuations in velocity, magnetic field, and density that have low frequencies compared with ion gyrofrequencies and are therefore well described by magnetohydrodynamics (MHD). Concisely summarized, neither the ratio of energy in inward "waves" to that in outward "waves", nor the ratio of kinetic to magnetic energy act as expected in WKB theory. Furthermore, additional observed features, including a temperature profile that is highly nonadiabatic, spectral power laws of the Kolmogoroff type, and the scaling of higher-order statistics, all require explanation. The presence and behavior of turbulence also relates to several other solar and heliospheric problems. For example, turbulence may be responsible for the heating source required in the lower corona to accelerate the wind, while observed scattering properties of energetic cosmic rays and solar energetic particles appear to favor types of spectral distribution of fluctuations associated with active turbulence cascade processes. Turbulence provides a natural if not entirely unique explanation for each of these observational properties. Taken together, the likely involvement of turbulence in explaining these issues becomes rather compelling. In this light, the requirement emerges to understand how, and, in physical terms, why turbulence is distributed in the heliosphere the way we observe it. This is particularly important if we are to understand the solar modulation of galactic cosmic rays, which propagate through regions of the interplanetary medium that have not yet been explored, and indeed may not be accessible for some time. The same set of issues bear on the understanding of the charged particle environment at any point in the heliosphere, including regions of importance in human and robotic exploration initiatives.

[3] In the present paper we address the issue of the distribution of MHD-scale turbulence in the heliosphere, employing an approach developed in recent years to explain observations such as the radial variation of temperature near the ecliptic, as observed by Voyager and Pioneer, and the observation of slow radial decay of highly Alfvénic states at high heliospheric latitudes by the Ulysses mission. As a natural extension of these efforts, we adopt the approximation that at any point in the supersonic and super-Alfvénic solar wind, information flows radially outward along the characteristics defined by the mean solar wind speed at that latitude. Consequently, by specifying the conditions at any angular coordinates at a fixed radius, one can determine the

[1]Department of Physics and Astronomy and Bartol Research Institute, University of Delaware, Newark, Delaware, USA.
[2]Department of Mathematics, University of Waikato, Hamilton, New Zealand.
[3]Institute for the Study of Earth, Oceans and Space, and Department of Physics, University of New Hampshire, Durham, New Hampshire, USA.

0148-0227/08/2007JA012711$09.00

turbulence properties at larger radius along the same angular direction. In this regard we seek to parameterize the latitudinally varying parameters and boundary conditions in the theory. Integrating outwards from these boundary conditions, we can provide a reasonable accounting of turbulence properties anywhere in a model heliosphere.

[4] Solar wind observations have been used to study MHD since the earliest observations were made [*Belcher and Davis Jr.*, 1971; *Coleman*, 1968, 1966]. Observations have shown evidence for both MHD waves [*Belcher and Davis Jr.*, 1971] and MHD turbulence [*Coleman*, 1968]. Close to the sun, strong correlations between the velocity and magnetic field are observed, typically associated with MHD Alfvén waves. As the solar wind advects outwards and evolves, a turbulence cascade operates to send energy to smaller scales where it is dissipated [*Matthaeus and Goldstein*, 1982; *Roberts et al.*, 1987a]. There is also evidence that the instability of large-scale sheared flows generates additional small-scale turbulence energy [*Roberts et al.*, 1992]. In this sense interplanetary turbulence experiences both expansion and driving as it evolves.

[5] Turbulence theory is primarily concerned with characterizing the fluctuations of the velocity and magnetic field that are superimposed upon the mean fields. These fluctuations can be measured by decomposing the fields as,

$$\mathbf{V} = \langle \mathbf{V} \rangle + \mathbf{v} \quad \text{and} \quad \mathbf{B} = \langle \mathbf{B} \rangle + \mathbf{b}, \tag{1}$$

with $\langle \cdots \rangle$ being some appropriate averaging operator; $\mathbf{v}$ and $\mathbf{b}$ are the fluctuating components. (Note that $\langle \mathbf{v} \rangle = \mathbf{0} = \langle \mathbf{b} \rangle$.) To make the decomposition more formal, one can introduce two spatial scales—a "fast" local scale $\mathbf{x}$ that measures rapid variations, e.g., at the turbulence scales, and a slow scale $\mathbf{r}$ that measures large-scale variations at the system inhomogeneity scale [*Marsch and Tu*, 1989; *Zhou and Matthaeus*, 1990a; *Marsch and Tu*, 1990a, 1990b; *Matthaeus et al.*, 1994b; *Tu and Marsch*, 1993]. In the usual way, we associate the averaging $\langle \cdots \rangle$ with averaging over the fast scale, so that for any function $F(\mathbf{r}, \mathbf{x})$, we require that the average $\langle F \rangle$ is a function only of $\mathbf{r}$. A corollary is that $\langle \partial F / \partial x_i \rangle \equiv 0$. Scale separation can be quantified by a small parameter, here $\epsilon = \lambda / r$ is suitable, where λ is the characteristic (correlation) scale of the turbulence, and r is the local heliocentric radial distance, taken to be of order the inhomogeneity scale. Gradients can then be expanded as $\nabla \rightarrow \nabla + \epsilon^{-1} \nabla_x$, where the operator $\nabla \equiv \nabla_r$ will now represent gradients at the slow, or transport scale. Typically $\varepsilon \ll 1$, e.g., at 1 AU in the interplanetary medium, $\lambda = 0.008$ AU [*Matthaeus et al.*, 2005].

[6] The small-scale fluctuations we consider are generated in the solar corona and also in situ by shear driving and by the turbulence cascade. They interact with one another in a highly nonlinear fashion. We treat λ as their characteristic scale, while keeping in mind that structure typically also exists at smaller scales, since the fluctuations frequently exhibit power law spectra within the inertial range (i.e., at scales $<\lambda$).

[7] Full modeling of the MHD turbulence present in the heliosphere would require solving the compressible MHD equations at all relevant scales, from the largest (an AU or so) down to the smallest scales where kinetic effects become important (about a proton gyroradius). Simulating such widely varying scales tends to be impractical. As such, other models are adopted.

[8] In this paper, we describe one such model that has been developed from the MHD equations over a period of years. The model incorporates known observational characteristics of the solar wind. We use the model to make large-scale predictions of turbulence distributions throughout the heliosphere. Such knowledge can be useful for understanding the heating of the solar wind, cosmic ray modulation and other problems. For convenience, we state the four main model equations here. These are radial transport equations for the energy, Z^2,

$$\frac{\mathrm{d}Z^2}{\mathrm{d}r} = -\frac{Z^2}{r} + \frac{C_{\mathrm{sh}} - M\sigma_D}{r} Z^2 + \frac{\dot{E}_{PI}}{U} - \alpha f^+ \frac{Z^3}{\lambda U}, \tag{2}$$

correlation scale, λ,

$$\frac{\mathrm{d}\lambda}{\mathrm{d}r} = \beta f^+ \frac{Z}{U} - \frac{\beta}{\alpha} \frac{\dot{E}_{PI}}{UZ^2} \lambda, \tag{3}$$

normalized cross helicity, σ_c,

$$\frac{\mathrm{d}\sigma_c}{\mathrm{d}r} = \alpha f' \frac{Z}{U\lambda} - \left[\frac{C_{\mathrm{sh}} - M\sigma_D}{r} + \frac{\dot{E}_{PI}}{UZ^2} \right] \sigma_c, \tag{4}$$

and (proton) temperature, T,

$$\frac{\mathrm{d}T}{\mathrm{d}r} = -\frac{4}{3} \frac{T}{r} + \frac{1}{3} \frac{m_p}{k_B} \frac{\alpha}{U} f^+ \frac{Z^3}{\lambda}. \tag{5}$$

In these equations, r is the heliocentric radius, U is the bulk solar wind velocity, C_{sh} represents the strength of the stream shear interactions, M is a geometry-dependent term reflecting the inhomogeneity and underlying turbulence symmetry, and $\ddot{\mathrm{E}}_{PI}$ relates to pickup proton interactions. The other quantities will be defined in section 2.

[9] In the following section we review the derivation and structure of these transport equations for turbulence in specified large-scale heliospheric fields. In section 3 we discuss details regarding the latitudinal variation of the inner boundary conditions, and the observationally based method we use to estimate the driving of turbulence by large-scale shear. Readers content to accept the model as given in equations (2)–(5) may wish to skip straight to section 4 where we present numerical solutions. The paper closes with our conclusions.

2. Derivation of the Model Equations

2.1. Scale Separation and Correlation Tensors

[10] The equations for our transport model can be derived from a two-scale analysis of the full set of MHD equations followed by a series of physically motivated approximations that are pertinent to the solar wind [*Matthaeus et al.*, 1994b, 1996, 2004; *Oughton and Matthaeus*, 1995; *Zhou and Matthaeus*, 1990a, 1990b; *Marsch and Tu*, 1989, 1990a, 1990b; *Tu and Marsch*, 1993; *Zank et al.*, 1996]. Previously, elements of the derivation of the model were found in a number of the above references. The lack of a completely coherent single treatment motivates us to provide here what

is essentially a complete derivation, all of the key approximations and the essential manipulations are assembled in the following subsections.

[11] We start by applying the decomposition described in equation (1) to the MHD equations. Next, we derive the evolution equations for the fluctuations, which are more conveniently expressed using the Elsässer variables, $\mathbf{z}^{\pm} \equiv \mathbf{v} \pm \mathbf{b}/\sqrt{4\pi\rho}$ [*Elsässer*, 1950], where ρ is the (proton) mass density. We obtain,

$$\frac{\partial \mathbf{z}^{\pm}}{\partial t} + (\mathbf{U} \mp \mathbf{V}_A)\cdot\nabla\mathbf{z}^{\pm} + \frac{1}{2}\nabla\cdot(\mathbf{U}/2 \pm \mathbf{V}_A)\mathbf{z}^{\pm} + \mathbf{z}^{\mp} \cdot\left[\nabla\mathbf{U} \pm \frac{\nabla\mathbf{B}_0}{\sqrt{4\pi\rho}} - \frac{I}{2}\nabla\cdot(\mathbf{U}/2 \pm \mathbf{V}_A)\right] = \mathbf{N}\mathbf{L}^{\pm} + \mathbf{S}^{\pm}, \quad (6)$$

where $\mathbf{U} \equiv \langle\mathbf{V}\rangle$, $\mathbf{B}_0 \equiv \langle\mathbf{B}\rangle$, $\mathbf{V}_A = \mathbf{B}_0/\sqrt{4\pi\rho}$, and I is the identity matrix. Note that $\mathbf{z}^{\pm}$ is a function of both the large-scale (i.e., solar wind scales) coordinates $\mathbf{r}$ and the small-scale (turbulence) coordinates $\mathbf{x}$. Local nonlinear effects, as well as source terms, are separated and represented by the terms $\mathbf{N}\mathbf{L}^{\pm}$ and $\mathbf{S}^{\pm}$, respectively, in anticipation of subsequent modeling. As is well-known, when the Elsässer fluctuations depend upon the coordinate parallel to the mean magnetic field, they can correspond to waves propagating along that field.

[12] Our goal is to develop a set of evolution equations for three turbulence quantities: (twice) the energy per unit mass, which in our usual notation is,

$$Z^2 = \frac{Z_+^2 + Z_-^2}{2} = \frac{\langle|\mathbf{z}^+|^2 + |\mathbf{z}^-|^2\rangle}{2} = \langle|\mathbf{v}|^2 + |\mathbf{b}|^2\rangle, \quad (7)$$

the normalized cross helicity

$$\sigma_c = \frac{H_c}{E} = \frac{Z_+^2 - Z_-^2}{Z_+^2 + Z_-^2}, \quad (8)$$

where $H_c = \langle\mathbf{v}\cdot\mathbf{b}\rangle$ is the actual cross helicity, and a similarity scale λ, which can be associated with a correlation scale of the turbulence, for example,

$$\lambda = \int_0^{\infty} R(\zeta,0,0)\,\mathrm{d}\zeta/R(0,0,0). \quad (9)$$

In the last equation R is the trace of any one of the turbulence correlation tensors, however, for specificity we take it to be the energy correlation tensor, $R = \langle\mathbf{v}\cdot\mathbf{v}' + \mathbf{b}\cdot\mathbf{b}'\rangle$. Here, the prime denotes evaluation at the lagged small-scale coordinate, e.g., $\mathbf{v}' = \mathbf{v}(\mathbf{r}, \mathbf{x} + \zeta)$; see below. At this point, the direction associated with the ζ-coordinate is arbitrary. The quantity λ is intended to describe the size of the largest correlated energy-containing eddies or magnetic structures that are associated with turbulence.

[13] Using equations (6), one can form equations for the evolution of all the independent second-order correlation functions that appear in incompressible MHD [*Oughton et al.*, 1997]. This is, however, more than we need to provide a derivation of a four-equation scalar model for the distribution of interplanetary turbulence. For this purpose we will follow the developments leading to two-equation treatments [*Zhou and Matthaeus*, 1990a; *Matthaeus et al.*, 1994a, 1996; *Zank et al.*, 1996], and will include temperature effects [*Matthaeus et al.*, 1999; *Smith et al.*, 2001], as well as cross helicity effects [*Matthaeus et al.*, 2004; *Breech et al.*, 2005].

[14] Before proceeding with the derivation we list the key approximations to be employed, in order of their application.

[15] 1. Scale separation;

[16] 2. Local incompressibility with specified large-scale time-steady density field;

[17] 3. Large-scale speed and magnetic field specified, with large-scale solar wind speed $U \gg V_A$, the large-scale Alfvén speed;

[18] 4. Assumption that large-scale gradients are in the radial direction;

[19] 5. Structural similarity of the correlations (meaning that each tensor element is separately proportional to the trace) and parameterization of the energy difference tensor;

[20] 6. Separation of the large-scale shear tensor and modeling of the symmetric part associated with expansion;

[21] 7. Assumption of a known fixed symmetry of the fluctuations (including neglect of magnetic helicities where needed);

[22] 8. Single similarity scale λ (which is identified with the correlation scale); and

[23] 9. Assumption that turbulent decay leads to proton heating.

[24] Taken together, approximations (I), and (IV) imply that a correlation function such as $R(\mathbf{r}, \zeta) = \langle v_i v_j'\rangle$, can be written as $R = u^2(r)\, f(\zeta)$ where r is the large-scale (slow) radial coordinate, u^2 is the slowly varying turbulence energy density, and f is a dimensionless correlation function that depends only on the small-scale separation vector ζ. In this way the scale-separated energy evolution can be seen as closely related to the principle of self-preservation of turbulence correlations introduced by *von Kármán and Howarth* [1938].

[25] With the above approximations, one uses the scale-separated MHD equations to form equations for just a few correlation functions, such as

$$R_{ij}^{\pm}(\mathbf{r},\boldsymbol{\zeta},t) = \langle z_i^{\pm}(\mathbf{r},\mathbf{x},t) z_j^{\pm}(\mathbf{r},\mathbf{x}+\boldsymbol{\zeta},t)\rangle = \langle z_i^{\pm} z_j^{\pm\prime}\rangle. \quad (10)$$

In the second form we use a $'$ to denote the lagged position $\mathbf{x} + \zeta$. (We assume that the magnetic field is in Alfvén speed units, that is $\mathbf{B} \rightarrow \mathbf{B}/\sqrt{4\pi\rho}$.). Hereafter, the $\mathbf{r}$ and t dependence of $\mathbf{z}^{\pm}$ and the correlations will often not be explicitly written.

[26] Starting from equation (6), we derive equations for the evolution of $R^{\pm}$. Ignoring terms of order V_A/U, we obtain,

$$\frac{\partial R_{ij}^{\pm}}{\partial t} + \mathbf{U}\cdot\nabla R_{ij}^{\pm} + R_{ij}^{\pm}\nabla\cdot\frac{\mathbf{U}}{2} + \Pi_{ij}^{\pm} = NL_{ij}^{\pm} + S_{ij}^{\pm}. \quad (11)$$

The right hand side includes a tensor $NL_{ij}^{\pm}$ that represents the local nonlinear terms, and another $S_{ij}^{\pm}$ that represents effects of sources. Models for these are developed separately. Note that except for the terms designated as Π_{ij} (see next paragraph), and possibly the nonlinear terms, the compo-

nents of the tensors R^{+}_{ij} and R^{-}_{ij} evolve independently of one another.

[27] The $\Pi^{\pm}_{ij}$ tensors in equations (11) require some detailed discussion. They represent inhomogeneous (but linear) effects on $\mathbf{z}^{+}$ due to $\mathbf{z}^{-}$, and vice versa. These terms have been referred to previously as mixing effects, or MECS, for "mixing, expansion, compression, and shear" effects [*Zhou and Matthaeus*, 1990a; *Zank et al.*, 1996; *Matthaeus et al.*, 1996]. This terminology refers to the fact that, at this order of approximation, these terms depend on the large-scale solar wind velocity shear tensor $\partial U_i/\partial r_j$. Since they correspond to couplings of the two Elsässer fields, they involve the cross correlation tensors,

$$\begin{aligned}\Lambda_{ij}(\boldsymbol{\zeta}) &= \langle z^{+}_i(\mathbf{x}) z^{-}_j(\mathbf{x}+\boldsymbol{\zeta})\rangle = \langle (v_i + b_i)\left(v'_j - b'_j\right)\rangle,\\ \tilde{\Lambda}_{ij}(\boldsymbol{\zeta}) &= \langle z^{+}_i(\mathbf{x}+\boldsymbol{\zeta}) z^{-}_j(\mathbf{x})\rangle = \langle \left(v'_i + b'_i\right)(v_j - b_j)\rangle.\end{aligned} \tag{12}$$

Note that Λ_{ij} and $\tilde{\Lambda}_{ij}$ are independent of $R^{\pm}_{ij}$, and that the combination $\hat{\Lambda}_{ij} = \Lambda_{ij} + \tilde{\Lambda}_{ji}$ is homogeneous in that it satisfies the elementary space translation symmetry property $\hat{\Lambda}_{ij}(\boldsymbol{\zeta}) = \hat{\Lambda}_{ji}(-\boldsymbol{\zeta})$, whereas Λ and $\tilde{\Lambda}$ separately do not. We can also write the Λ tensors in terms of the energy difference tensor, $R^{D}_{ij} = \langle v_i v'_j - b_i b'_j\rangle$, the difference between the velocity and magnetic autocorrelation functions, and a cross correlation tensor, $R^{vb-}_{ij} = \langle v_i b'_j - v'_j b_i\rangle$. The antisymmetric part of this cross correlation tensor is $R^{vb-a}_{ij}(\zeta) = -\epsilon_{ijm} F_m(\zeta)$, where $F_m(\zeta = 0) = \langle (\mathbf{v}\times\mathbf{b})_m\rangle$. For reasons that are apparent this can be described as the induced electric field correlation tensor.

[28] In terms of these tensors we may identify that

$$\Lambda_{ij} = R^{D}_{ij} - R^{vb-}_{ij} \qquad \text{and} \qquad \tilde{\Lambda}_{ij} = R^{D}_{ji} + R^{vb-}_{ji}. \tag{13}$$

Using these we obtain explicit expressions for the mixing terms,

$$\begin{aligned}\Pi^{+}_{ij} &= \Lambda_{ik}\frac{\partial U_j}{\partial r_k} + \tilde{\Lambda}_{jk}\frac{\partial U_i}{\partial r_k} - \frac{1}{2}\left(\Lambda_{ij} + \tilde{\Lambda}_{ji}\right)\nabla\cdot\frac{\mathbf{U}}{2},\\ \Pi^{-}_{ij} &= \Lambda_{kj}\frac{\partial U_i}{\partial r_k} + \tilde{\Lambda}_{ki}\frac{\partial U_j}{\partial r_k} - \frac{1}{2}\left(\Lambda_{ij} + \tilde{\Lambda}_{ji}\right)\nabla\cdot\frac{\mathbf{U}}{2}.\end{aligned} \tag{14}$$

[29] The equations simplify if we are concerned with the evolution of the trace of the correlation functions. In particular, the trace of the $\Pi^{\pm}$ terms can be written

$$\begin{aligned}\Pi^{\pm}_{ii} &= \left(R^{D}_{ik} \mp R^{vb-}_{ik}\right)\frac{\partial U_i}{\partial r_k} + \left(R^{D}_{ki} \pm R^{vb-}_{ki}\right)\frac{\partial U_i}{\partial r_k} - R^{D}_{ii}\nabla\cdot\frac{\mathbf{U}}{2}\\ &= 2\left(R^{Ds}_{ik} \mp R^{vb-a}_{ik}\right)\frac{\partial U_i}{\partial r_k} - R^{Ds}_{ii}\nabla\cdot\frac{\mathbf{U}}{2},\end{aligned} \tag{15}$$

where R^{Ds}_{ij} is the symmetric part of R^{D}_{ij}.

[30] In the following four subsections we show how physically motivated and/or observationally supported assumptions can be used to simplify the linear terms in equation (11).

2.1.1. Shear and Expansion Tensor

[31] At this point in the derivation, it is useful to discuss the structure of the fully contracted tensors that appear on the right hand side of equation (15). Suppose that the large-scale shear tensor is separated into symmetric and antisymmetric parts,

$$\begin{aligned}\frac{\partial U_i}{\partial r_j} &= \Omega^{s}_{ij} + \Omega^{a}_{ij}, \Omega^{s}_{ij} = \frac{1}{2}\left(\frac{\partial U_i}{\partial r_j} + \frac{\partial U_j}{\partial r_i}\right),\\ \Omega^{a}_{ij} &= \frac{1}{2}\left(\frac{\partial U_i}{\partial r_j} - \frac{\partial U_j}{\partial r_i}\right)\end{aligned} \tag{16}$$

[32] For the case that the large-scale flow is a simple spherical expansion at constant speed U, one finds that $\Omega^{s}_{ij} = (U/r)(\delta_{ij} - \hat{r}_i\hat{r}_j)$ and $\Omega^{a}_{ij} = 0$, where $\hat{\mathbf{r}}$ is a unit vector in the outward radial direction. We also see that $\nabla\cdot\mathbf{U} = 2U/r$. Combining these results yields (summation over repeated indices is implied)

$$\Pi^{\pm}_{ii}(\mathbf{r},\boldsymbol{\zeta}) = \frac{U}{r}R^{Ds}_{ij}(\boldsymbol{\zeta})\left(\delta_{ij} - 2\hat{r}_i\hat{r}_j\right). \tag{17}$$

There is no contribution here due to the electric field correlation tensor, since the full contraction of an antisymmetric tensor and a symmetric tensor vanishes.

[33] Of course, additional contributions to Ω^{s} and Ω^{a}, say Ω'^{s} and Ω'^{a}, will arise from stream interactions, shocks, and other departures from uniform spherical expansion. These effects are modeled separately; see section 2.1.5.

2.1.2. Energy Difference Closure

[34] The presence of the energy difference tensor in equation (11) [via equation (17)] presents a type of closure problem. Specifically, the evolution of $R^{\pm}$ involves R^{D}, and the equation for its evolution (not shown here) involves still additional independent quantities leading to the possibility of 16 coupled tensor equations [*Oughton et al.*, 1997], each of which requires modeling of a nonlinear term. It is a considerable simplification if this set can be truncated by a closure approximation.

[35] To this end we first observe that for the trace at zero lag, we have *exactly*

$$R^{Ds}_{ii}(0) = \langle \mathbf{v}\cdot\mathbf{v} - \mathbf{b}\cdot\mathbf{b}\rangle\frac{R_{ii}(0)}{R_{jj}(0)} = \sigma_D R_{ii}(0), \tag{18}$$

where the total (velocity plus magnetic) correlation tensor is

$$R_{ij}(\boldsymbol{\zeta}) \equiv \frac{R^{+}_{ij} + R^{-}_{ij}}{2} = \langle v_i v'_j + b_i b'_j\rangle, \tag{19}$$

and $\sigma_D = \langle v^2 - b^2\rangle/\langle v^2 + b^2\rangle$ is the normalized energy difference. If σ_D is known, or modeled, a closure between $R^{Ds}_{ii}(0)$ and $R_{ii}(0)$ is obtained. This motivates trying to find a similar closure for the complete tensor.

[36] We employ the *structural similarity* approximation, wherein each element of a correlation tensor is assumed to be proportional to the trace of the same tensor [*Tennekes and Lumley*, 1972; *Townsend*, 1976; *Zank et al.*, 1996]. For example, $R^{Ds}_{ij}(\zeta) \approx d_{ij}\langle \mathbf{v}\cdot\mathbf{v}' - \mathbf{b}\cdot\mathbf{b}'\rangle$, where the d_{ij} are the (order unity) proportionality constants of the approximation.

Thus multiplying by one in a useful form, we obtain (no implied summations),

$$R_{ij}^{Ds}(\boldsymbol{\zeta}) = R_{ij}^{Ds}\frac{R_{ij}}{R_{ij}} \approx \frac{d_{ij}\langle \mathbf{v}\cdot\mathbf{v}' - \mathbf{b}\cdot\mathbf{b}'\rangle}{c_{ij}\langle \mathbf{v}\cdot\mathbf{v}' + \mathbf{b}\cdot\mathbf{b}'\rangle}R_{ij}(\boldsymbol{\zeta}) \approx_D R_{ij}(\boldsymbol{\zeta}). \tag{20}$$

In obtaining this last equation we have assumed that each $d_{ij}/c_{ij} \approx 1$. More importantly, we have approximated $\sigma_D(\boldsymbol{\zeta})$ by its value at zero lag, σ_D. This amounts to assuming that the energy difference correlation and the energy correlation fall off at about the same rate. Making the further approximation that σ_D = constant (with respect to r) yields $R_{ij}^{Ds} \propto R_{ij}$ and thus provides a closure. As is well known, constant σ_D implies that the ratio of kinetic to magnetic energy, the Alfvén ratio $r_A = \langle v^2\rangle/\langle b^2\rangle \equiv (1+\sigma_D)/(1-\sigma_D)$, is also a constant. We will apply this approximation to the terms involved in spherical expansion.

2.1.3. Rotational Symmetry of the Fluctuations

[37] When computing the trace of $R_{ij}^{\pm}$, information about the rotational symmetry (or, polarization) of the fluctuations is obscured. However, this is not so with regard to the time-evolution of $R_{ij}^{\pm}$. In equation (15), the trace of the mixing terms involves the full contraction of R_{ij}^{Ds} with the velocity shear tensor. Therefore all components may enter. Furthermore, even when the only nonuniformity is a simple spherical expansion, there is a preferred direction (the radial), and the component structure of the fluctuations enters the calculation. All such complications could be accommodated in a straightforward approach that solves separate equations for each of the Cartesian components of the correlation tensors, such as $R_{11}^{\pm}$, $R_{22}^{\pm}$, and $R_{33}^{\pm}$. However, this would add considerable complexity to the model due to the larger number of transport equations to be solved. However, more importantly such an approach would require that we separately model the nonlinear effects on a component-by-component basis. We view this as a prohibitive impediment, since the simple turbulence models we wish to employ are written most readily in terms of the total energy in all three components, and such simple models are not available for individual component energies.

[38] Instead, here (and in other recent transport applications) we adopt the approximation of a fixed specified turbulence symmetry. There are two basic choices we have studied:

(1) *isotropic symmetry*, in which the symmetric part of the correlation tensors is written

$$R_{ij}^{\pm} = \frac{R_{kk}^{\pm}}{3}\delta_{ij}, \tag{21}$$

and (2) *transverse symmetry*, in which

$$R_{ij}^{\pm} = \frac{R_{kk}^{\pm}}{2}\left(\delta_{ij} - \hat{B}_i\hat{B}_j\right), \tag{22}$$

where $\hat{\mathbf{B}}$ is the local large-scale magnetic field direction. At this level of description the transverse case can equally well apply to *axisymmetric slab* "*turbulence*", in which all wave vectors are parallel to $\hat{\mathbf{B}}$, or *axisymmetric two dimensional turbulence* (2D) in which all the turbulence wave vectors are perpendicular to $\hat{\mathbf{B}}$. In both these cases, $\mathbf{b}\cdot\hat{\mathbf{B}} = 0$. To simplify matters, we are writing the correlation tensors as symmetric—that is, we ignore the possibility of an antisymmetric part that is associated with magnetic helicity (for the slab and isotropic cases).

[39] Evaluating at zero lag yields the variance tensors. Thus for the isotropic case $R_{ij}^{\pm}(\boldsymbol{\zeta}=\mathbf{0}) = (Z_{\pm}^2/3)\delta_{ij}$, while for the transverse case $R_{ij}^{\pm}(\boldsymbol{\zeta}=\mathbf{0}) = (Z_{\pm}^2/2)\,(\delta_{ij} - \hat{B}_i\,\hat{B}_j)$.

[40] The assumption of fixed turbulence symmetry is justified by postulating that the local nonlinear turbulence effects are strong enough to enforce the chosen symmetry, acting at a timescale faster than the corresponding transport timescales. Typically the turbulence timescale is of order $\tau_{\rm nl} = \lambda/Z$, while expansion effects occur in a time of order $\tau_{\rm exp} = r/U$. Thus we require $\tau_{\rm nl} < \tau_{\rm exp}$ and the chosen symmetry might be enforced if the fluctuation scales of interest satisfy $\lambda < (Z/U)\,r$. This is usually satisfied for interplanetary fluctuations; for example, at $r = 1$ AU "worst case" values are $\lambda \sim 0.01$ AU with $Z \sim 200$ km/s.

2.1.4. Mixing Terms for Spherical Expansion

[41] Combining the results of the last three subsections, we can employ spherical expansion, energy difference closure, and fixed turbulence symmetry to evaluate the mixing terms.

[42] Inserting either equation (21) or equation (22) into equation (20) and substituting into equation (17) we find that for the isotropic case,

$$\Pi_{ii}^{\pm} = \frac{U}{r}\frac{\sigma_D R_{kk}}{3}\delta_{ij}\left(\delta_{ij} - 2\hat{r}_i\hat{r}_j\right), \tag{23}$$

and in the transverse cases,

$$\Pi_{ii}^{\pm} = \frac{U}{r}\frac{\sigma_D R_{kk}}{2}\left(\delta_{ij} - \hat{B}_i\hat{B}_j\right)\left(\delta_{ij} - 2\hat{r}_i\hat{r}_j\right). \tag{24}$$

These can be written compactly as

$$\Pi_{ii}^{\pm} = M\sigma_D\frac{U}{r}R_{ii}, \tag{25}$$

where M is determined by the turbulence symmetry. For the cases we have discussed so far,

$$M = \begin{cases} 1/3, & \text{isotropic} \\ \cos^2\psi, & \text{transverse.} \end{cases} \tag{26}$$

for $\psi = \cos^{-1}(\hat{\mathbf{B}}_0\cdot\hat{\mathbf{r}})$ the winding angle between the mean magnetic field and the radial direction, and we recall that $R_{ij} = (R_{ij}^{+} + R_{ij}^{-})/2$.

2.1.5. Accounting for Shear Effects

[43] At this point in the derivation, the equation for $R_{ii}\,(\zeta)$ is

$$\frac{\partial}{\partial t}R_{ii} + U\frac{\partial}{\partial r}R_{ii} + \frac{U}{r}R_{ii} + M\sigma_D\frac{U}{r}R_{ii} + (shear) = NL_{ii} + S_{ii}. \tag{27}$$

We now seek to model the effects of shear driving. Large-scale shear stresses affect the turbulence by "deforming"

turbulent structures. This deformation work has the effect of transferring energy from the large scales to the turbulent scales [e.g., *Tennekes and Lumley*, 1972]. Thus shear helps drive the turbulence by supplying energy from the large scales. This driving, however, usually occurs in an anisotropic fashion and can destroy the underlying turbulent symmetries.

[44] The shear terms arise from the contraction of R_{ik}^{Ds} with the large-scale shear tensor. Since R^{Ds} is symmetric, only the symmetric part of the shear tensor, Ω_{ik}^{s}, gives rise to shearing effects. The antisymmetric part of the shear tensor couples with the R^{vb-a} tensor; we neglect these couplings since R^{vb-a} relates to the mean values of the induced electric field, which tend to be small in the solar wind [*Breech et al.*, 2003]. As seen in section 2.1.1, the diagonal elements of $\Omega_{ik}^{s} = \Omega^{0s} + \Omega'^{s}$ are associated with expansion effects. The off-diagonal elements contain the shearing effects and increase the turbulence energy. For simplicity, we assume that shear driving acts at all scales in such a way as to maintain the same spectral shape.

[45] We model the shear effects as

$$(shear) = R_{ik}^{Ds}\Omega_{ik}^{'s} \sim R_{ii}\frac{\Delta U}{\Delta r} \sim C_{\rm sh}R_{ii}\frac{U}{r}, \tag{28}$$

where $C_{\rm sh}$ represents the strength of the shear interaction which changes U by ΔU over a distance of Δr. Interpreting this shear model must be done very carefully. For the most part, the solar wind velocity is constant along radial spokes [*McComas et al.*, 2000], but it varies latitudinally, which allows for shear to develop. The Δr in equation (28) is the distance associated with large-scale velocity changes. These changes occur mainly with varying latitudes. We expect this distance to scale like r owing to expansion as the streams progress outward.

[46] Equation (27) now becomes

$$\frac{\partial}{\partial t}R_{ii}(\boldsymbol{\zeta}) + U\frac{\partial}{\partial r}R_{ii} + \frac{U}{r}R_{ii} + M\sigma_D\frac{U}{r}R_{ii} - C_{\rm sh}\frac{U}{r}R_{ii} = NL_{ii} + S_{ii}, \tag{29}$$

where a minus was placed on the shear term to ensure that it adds energy.

2.2. Reduction to Scalar Equations

[47] We are now in a position to derive equations for the total energy and the similarity (correlation) length scale, by assuming steady state conditions and manipulating equation (29). First, evaluating equation (29) at zero lag leads to the equation for the total turbulence energy, Z^2,

$$U\frac{{\rm d}Z^2}{{\rm d}r} + \frac{U}{r}Z^2 + \frac{M\sigma_D - C_{\rm sh}}{r}UZ^2 = NL_Z + S_Z. \tag{30}$$

[48] Second, integrating equation (29) over all possible lags leads to the equation for the similarity scale, λ. We define

$$L \equiv \int_0^\infty R_{ii}(\zeta, 0, 0)\,{\rm d}\zeta = Z^2\lambda. \tag{31}$$

In this definition we have arbitrarily chosen a coordinate system in which the $\hat{1}$ direction defines the correlation length of interest. Note that our purpose is to choose an integral scale that measures the size of the dynamically important turbulence structures, so that we can apply an MHD phenomenology of similar structure to the (pre-Kolmogoroff) self-preservation of *von Kármán and Howarth* [1938]. As is also done in hydrodynamics, we elect to associate the similarity scale with one of the integral, or outer, scales of the turbulence [e.g., *Batchelor*, 1970]. Since several (related) scales of this type exist even in isotropic turbulence, there must remain some modest ambiguity in the theory. Furthermore, other scales are available in the (anisotropic) solar wind, e.g., the characteristic integral length scales associated with different directions of integration, and with the different fluctuation fields $\mathbf{z}^+$ and $\mathbf{z}^-$. To resolve these difficulties, we adopt a single similarity scale, specifically one that is representative of the energy-containing scale of the dominant fluctuations. This is discussed further in section 2.3. Observational difficulties also arise and will be discussed below.

[49] To summarize this point, we have assumed that there is a single correlation scale, λ, rather than separate scales for outward and inward fluctuations. We can interpret λ as the scale near which most of the fluctuation energy resides.

[50] Integrating equation (29) with respect to ζ gives

$$U\frac{{\rm d}L}{{\rm d}r} + \frac{U}{r}L + \frac{M\sigma_D - C_{\rm sh}}{r}UL = NL_L + S_L. \tag{32}$$

The evolution equation for λ is obtained by multiplying equation (30) by λ, subtracting the resulting equation from equation (32), and using equation (31) to eliminate L. This yields the remarkably simple form

$$U\frac{{\rm d}\lambda}{{\rm d}r} = NL_\lambda + S_\lambda. \tag{33}$$

[51] Finally, we can also obtain an equation for the transport of cross helicity, expressed in terms of the normalized cross helicity, σ_c, defined as

$$\sigma_c = \frac{Z_+^2 - Z_-^2}{Z_+^2 + Z_-^2} \tag{34}$$

The first step is to construct the evolution equation for

$$R_{ij}^{\sigma_c} = \frac{1}{2}\left(R_{ij}^{+} - R_{ij}^{-}\right). \tag{35}$$

Taking the difference of equations (11), and applying the assumptions given above leads to

$$U\frac{\rm d}{{\rm d}r}R_{ii}^{\sigma_c} + \frac{U}{r}R_{ii}^{\sigma_c} = NL_{ii} + S_{ii}. \tag{36}$$

[52] Evaluating this at zero lag yields

$$U\frac{\rm d}{{\rm d}r}\left(Z^2\sigma_c\right) + Z^2\sigma_c\frac{U}{r} = NL + S. \tag{37}$$

Multiplying equation (30) by σ_c and subtracting the resulting equation from equation (37) produces the desired equation:

$$U\frac{\mathrm{d}\sigma_c}{\mathrm{d}r} - \frac{M\sigma_D - C_{\mathrm{sh}}}{r}U\sigma_c = NL_{\sigma_c} + S_{\sigma_c}. \tag{38}$$

[53] Similar to our approach with λ, we could also integrate equation (36) over all possible lags to obtain a cross-helicity correlation scale. However, due to the assumptions applied, this procedure leads to the same equation as equation (38), consistent with our approximation of a single similarity scale.

2.3. Modeling Local Nonlinearities

[54] In order to complete the transport model, we must specify forms for the nonlinear terms. Source terms, particularly driving from pickup proton interactions, will be discussed later. To model the nonlinear terms, we examine the homogeneous case, e.g., we ignore shear driving and mixing effects.

[55] A useful starting point is to assume $\sigma_c = 0$ and adopt a model analogous to a von Kármán-Taylor model for hydrodynamic decay. This leads to the following model for energy decay,

$$\frac{\mathrm{d}Z^2}{\mathrm{d}t} = -\alpha\frac{Z^2}{\tau_{\mathrm{nl}}} = -\alpha\frac{Z^3}{\lambda}, \tag{39}$$

along with

$$\frac{\mathrm{d}\lambda}{\mathrm{d}t} = \beta\frac{\lambda}{\tau_{\mathrm{nl}}} = \beta Z, \tag{40}$$

where $\tau_{\mathrm{nl}} = \lambda/Z$ is the eddy-turnover time and α, β are constants of order unity.

[56] We can generalize this model for nonzero cross helicity and write, based on analysis of the MHD equations [*Dobrowolny et al.*, 1980; *Matthaeus et al.*, 1994a; *Hossain et al.*, 1995],

$$\frac{\mathrm{d}Z_\pm^2}{\mathrm{d}t} = -\frac{\alpha_\pm}{\lambda_\pm}Z_\pm^2 Z_\mp \rightarrow -\frac{\alpha}{\lambda}Z_\pm^2 Z_\mp, \tag{41}$$

where we once again do not distinguish between similarity length-scales that appear in the two equations. Upon using the identities $Z_\pm^2 = (1 \pm \sigma_c)Z^2$ we find immediately that

$$\frac{\mathrm{d}Z^2}{\mathrm{d}t} = -\alpha f^+(\sigma_c)\frac{Z^3}{\lambda}, \tag{42}$$

where we define

$$f^\pm(\sigma_c) = \frac{\left(1-\sigma_c^2\right)^{1/2}}{2}\left[(1+\sigma_c)^{1/2} \pm (1-\sigma_c)^{1/2}\right]. \tag{43}$$

[57] This Kármán–Taylor phenomenology ignores Alfvén propagation effects and is most appropriate when the strongest nonlinearities are those associated with anisotropic quasi–two-dimensional (quasi-2D or reduced) MHD. The paradigm for this is "2D" turbulence, where wave vectors are perpendicular to $\mathbf{B}_0$, i.e., $k_\parallel \equiv 0$, and there is no Alfvén propagation effect at all.

[58] For nonlinear evolution of the correlation scale we recall from equation (31) that $L \equiv (\lambda_+ Z_+^2 + \lambda_- Z_-^2)/2 = Z^2\lambda$, and thus temporarily restore two length-scales $\lambda_\pm$. Carrying out a time derivative on this definition and using the approximation $\lambda_+ = \lambda_- = \lambda$, we find

$$\frac{\mathrm{d}\lambda}{\mathrm{d}t} = \frac{Z_+^2\dot{\lambda}_+ + Z_-^2\dot{\lambda}_-}{2Z^2}, \tag{44}$$

where an overdot designates a time derivative. We now employ a finite-H_c generalization of equation (40) suggested by *Hossain et al.* [1995], namely that $\lambda_\pm \sim Z_\mp$, and arrive at $\dot{\lambda} = \beta(Z_+^2 Z_- + Z_-^2 Z_+)/(2Z^2) = -\beta\alpha^{-1}\lambda Z^{-2}\mathrm{d}Z^2/\mathrm{d}t$, for some constant β. Using equation (42) this becomes,

$$\frac{\mathrm{d}\lambda}{\mathrm{d}t} = \beta f^+(\sigma_c)Z, \tag{45}$$

which is our required generalization of equation (40).

[59] The equation for evolution of σ_c is obtained from differentiating equation (34),

$$\frac{\mathrm{d}\sigma_c}{\mathrm{d}t} = \frac{\dot{Z}_+^2 - \dot{Z}_-^2}{2Z^2} - \frac{\sigma_c}{Z^2}\frac{\mathrm{d}Z^2}{\mathrm{d}t}, \tag{46}$$

and then using equations (41) and (42) to arrive at

$$\frac{\mathrm{d}\sigma_c}{\mathrm{d}t} = \alpha\frac{Z}{\lambda}[\sigma_c f^+(\sigma_c) - f^-(\sigma_c)], \tag{47}$$

where $f^\pm$ are as defined in equation (43). The behavior of $f^\pm(\sigma_c)$ versus σ_c is more fully described by *Matthaeus et al.* [2004]. Note that the square bracketed term in equation (47), always has the same sign as σ_c, and thus this equation, for decaying MHD turbulence *always* amplifies a seed cross helicity. This dynamical effect has been called "dynamic alignment" [*Dobrowolny et al.*, 1980; *Grappin et al.*, 1982; *Matthaeus et al.*, 1983; *Pouquet et al.*, 1986], since it favors production of Alfvénic (correlated) velocity and magnetic field fluctuations. However, solar wind turbulence typically does not display this effect, but rather shows reduction of Alfvénicity as turbulence ages with increasing heliocentric distance. This is connected with driving sources.

[60] The three equations (42), (45), and (47) provide a phenomenological description of turbulent decay of homogeneous MHD turbulence with cross helicity. Although equivalent to the formulation by *Hossain et al.* [1995], as written here it is evident that the effect of nonzero cross helicity can be thought of as a reduction in the effective decay constants, i.e., $\alpha \rightarrow \alpha f^+(\sigma_c)$ and $\beta \rightarrow \beta f^+(\sigma_c)$, due to the associated weakening of the nonlinear couplings as $\mathbf{v}$ and $\mathbf{b}$ become more correlated.

2.4. A Four-Equation Model of Interplanetary Turbulence

[61] Combining the results of the previous two sections, we obtain a model for interplanetary turbulence transport:

$$\frac{\mathrm{d}Z^2}{\mathrm{d}r} = -\frac{Z^2}{r} + \frac{C_{\mathrm{sh}} - M\sigma_D}{r} Z^2 - \frac{\alpha f^+(\sigma_c)}{\lambda U} Z^3, \tag{48}$$

$$\frac{\mathrm{d}\lambda}{\mathrm{d}r} = \frac{\beta f^+(\sigma_c)}{U} Z, \tag{49}$$

$$\frac{\mathrm{d}\sigma_c}{\mathrm{d}r} = -\frac{C_{\mathrm{sh}} - M\sigma_D}{r}\sigma_c + \frac{\alpha f'(\sigma_c)}{U\lambda} Z, \tag{50}$$

where we have defined $f'(\sigma_c) = \sigma_c f^+(\sigma_c) - f^-(\sigma_c)$.

[62] In addition to these three equations, a temperature equation is added to the model,

$$\frac{\mathrm{d}T}{\mathrm{d}r} = -\frac{4}{3}\frac{T}{r} + \frac{1}{3}\frac{m_p}{k_B}\frac{\alpha}{U} f^+(\sigma_c)\frac{Z^3}{\lambda}. \tag{51}$$

In this equation, there is a source of internal energy added to the right hand side, sometimes called a ''heating function'', which is just the negative of the energy lost to the turbulence through cascade and dissipation, embodied here by the assumed von Kármán-type decay rate proportional to Z^3/λ.

[63] Apart from terms representing pickup proton effects (see the next section), these equations are almost identical to those used in previous studies [*Matthaeus et al.*, 1999, 2004; *Smith et al.*, 2001, 2006; *Isenberg*, 2005; *Breech et al.*, 2005]. The difference between those studies and this work is the similarity scale transport, equation (49), in which shear and mixing terms do not appear. This is the result of using a different closure for R_{ij}^{Ds}. The previous studies assumed $\int R_{ij}^{Ds}(\zeta)\, \mathrm{d}\zeta = 0$, which implies that the areas under the curves of $\langle v_i v'_j \rangle$ and $\langle b_i b'_j \rangle$ are equal. This corresponds to shear driving and mixing at scales larger than λ. In contrast, for this work we adopted a different strategy and have applied structural similarity, equation (20), early in the calculation. Physically, this corresponds to shear driving and mixing at all scales (e.g., injecting energy without changing the shape of the spectrum).

[64] In the next section, we supplement these equations with terms representing pickup proton effects, $\dot{E}_{PI}/U$ [*Williams et al.*, 1995; *Zank et al.*, 1996; *Isenberg et al.*, 2003; *Isenberg*, 2005].

2.5. Pickup Protons

[65] In the outer parts of the heliosphere, the solar wind interacts with neutral particles slowly flowing in from the interstellar medium (ISM). These neutral particles, primarily hydrogen, can be ionized by solar UV radiation or by charge exchange with the solar wind protons. Once ionized, these interstellar particles initially stream through the solar wind plasma at the solar wind speed, and gyrate around the local magnetic field with perpendicular speeds on the order of U. These ''pickup protons'' are then scattered toward isotropy by the inertial range turbulent fluctuations. The pickup protons lose some energy in this scattering process, generating waves which act as an extended driving source for the turbulence.

[66] The rate at which this energy is added is proportional to the creation rate of new pickup protons, N/τ_{ion}, where N is the local interstellar hydrogen density and τ_{ion} is the neutral ionization time at 1 AU, taken to be 10^6 s [*Smith et al.*, 2001]. For a cold interstellar gas streaming into a steady spherical heliosphere, the ionization time increases as r^2 and the resulting neutral hydrogen density is given by

$$N = n_h \exp(-L_{\mathrm{cav}}/r), \tag{52}$$

where $n_h = 0.1$/cc is the density of the inflowing hydrogen at the solar wind termination shock and L_{cav} is the scale of the ionization cavity around the Sun, taken to be $L_{\mathrm{cav}} = 8.0$ AU. The fraction of pickup proton kinetic energy transferred into waves through the isotropization process scales roughly as V_A/U [*Isenberg et al.*, 2003; *Isenberg*, 2005], so we approximate the pickup proton source term in the turbulent energy equation as

$$\frac{\dot{E}_{PI}}{U} = \frac{f_D V_A n_h}{n_{\mathrm{sw}}\tau_{\mathrm{ion}}} \exp(-L_{\mathrm{cav}}/r), \tag{53}$$

where n_{sw} is the solar wind density at 1 AU and f_D accounts for the kinetic details of the isotropization. In principle, f_D is a function of V_A/U and of the properties of the inertial range spectra, so it will depend on heliocentric position and solar cycle phase [*Smith et al.*, 2006]. f_D can be eliminated by postulating that the turbulent cascade restricts the amount of self-generated wave energy available for scattering the pickup protons [*Isenberg et al.*, 2003; *Isenberg*, 2005; *Smith et al.*, 2006]. The rate of energy added is then dependent on the turbulent fluctuation amplitude, but is less dependent on the self-generated wave-energy. This yields good agreement with observations [*Smith et al.*, 2006], and provides clear evidence for the operation of a turbulent cascade, but is beyond the scope of the current work. For the purposes of this investigation, focused on the large scale turbulence distributions, we set a constant $f_D = 0.25$. This value falls within the range of acceptable values that yield good observational agreement.

[67] We should note that this model for the pickup proton interaction assumes spherically symmetry, particularly the neutral hydrogen density in equation (52). The neutral hydrogen primarily flows into the heliosphere along the ecliptic plane from the direction coinciding with the ''nose'' of the heliosphere. Equation (52) can be corrected to account for this [*Williams et al.*, 1995; *Smith et al.*, 2006]. However, in keeping with other portions of the model, we will use the spherically symmetric forms. In the outer heliosphere, the error caused by this choice is small, <10%. The error increases in the inner heliosphere, but there the pickup proton effects are overwhelmed by shear effects.

[68] We then include the pickup proton driving by modifying the model equations (48)–(51), to add energy at the rate given by equation (53). The energy becomes

$$\frac{\mathrm{d}Z^2}{\mathrm{d}r} = -\frac{Z^2}{r} + \frac{C_{\mathrm{sh}} - M\sigma_D}{r} Z^2 + \frac{\dot{E}_{PI}}{U} - \frac{\alpha f^+(\sigma_c)}{\lambda U} Z^3. \tag{54}$$

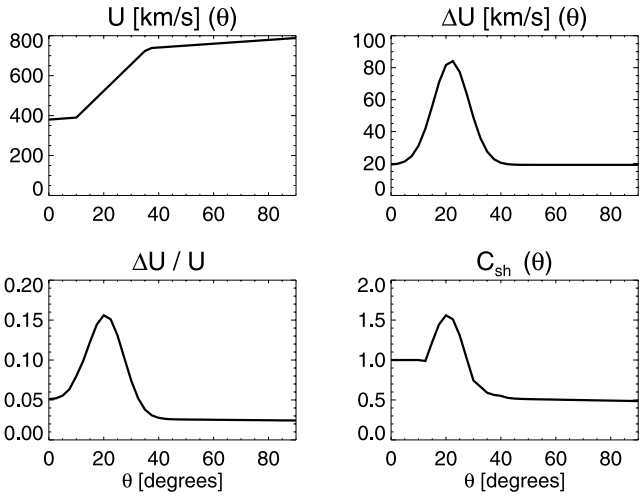

Figure 1. Latitudinal profiles for velocity and C_{sh} used for running the transport model. The U and ΔU profiles are obtained from Ulysses measurements [*McComas et al.*, 2000], and are treated as being independent of r.

[69] Pickup protons drive the turbulence at high wave numbers, e.g., in the inertial range. The interaction can thus "drag" the correlation scale toward smaller scales (higher wave number). As the pickup protons effectively decrease λ, we write

$$\frac{d\lambda}{dr} = \frac{\beta f^{+}(\sigma_c)}{U} Z - \frac{\beta}{\alpha} \frac{\dot{E}_{PI}}{UZ^2} \lambda. \tag{55}$$

[70] Finally, as pickup protons provide a source of driving for the turbulence, we expect them to interact with σ_c in a similar fashion to the driving by shear and mixing. We obtain

$$\frac{d\sigma_c}{dr} = \frac{\alpha f'(\sigma_c)}{U\lambda} Z - \left[\frac{C_{sh} - M\sigma_D}{r} + \frac{\dot{E}_{PI}}{UZ^2} \right] \sigma_c. \tag{56}$$

[71] There is no direct modification to the temperature equation, since the pickup proton interaction affects the turbulence at scales larger than the dissipation scales. Thus we expect no direct heat deposition due to the pickup protons, although they do cause indirect heating via their driving of the turbulence. This completes the derivation of the model equations.

2.6. List of Model Inputs

[72] Equations (2)–(5) form our turbulence transport model. Included in the model is driving through stream shear interactions (C_{sh}), mixing of outgoing and incoming Alfvénic fluctuations and expansion effects ($M\sigma_D$), and wave interactions due to pickup protons ($\ddot{E}_{PI}$ terms).

[73] In order to numerically solve the model equations we must specify values for the four dependent variables, Z^2, λ, σ_c, and T at some inner boundary, along with the various model parameters. The latter include,

[74] •The Kármán–Taylor constants, α and β. These should be of order unity and here we use $\alpha = 2\beta = 0.8$.

[75] •The strength of the shear interaction, C_{sh}, and the underlying turbulence symmetry, M.

[76] •The solar wind speed, U.

[77] •For the pickup protons we also require the Alfvén speed, V_A, and the latitudinal density profile at 1 AU. The Alfvén speed is set by adopting a Parker spiral model for the background magnetic field and specifying that $\rho \sim 1/r^2$.

[78] Choices for the other parameters and initial values are discussed in the next section.

3. Selecting Parameters and Boundary Data

3.1. Estimating C_{sh}

[79] In the inner parts of the heliosphere (8AU), shear is the dominant driving source. At lower latitudes, the shear arises from corotating interaction regions (CIRs) [*Burlaga*, 1974; *Smith and Wolfe*, 1976] while at higher latitudes the shear is primarily due to microstreams [*Neugebauer et al.*, 1995]. The parameter C_{sh} is used to model the effects of the stream shear interactions, as discussed in section 2.1.5. Specifically, from equation (28), we model it as

$$C_{sh} = \frac{\Delta U}{U} \frac{r}{\Delta r}. \tag{57}$$

Estimates for ΔU and U can be determined directly through observations [*McComas et al.*, 2000]. The top two panels of Figure 1 show latitude profiles for U and ΔU derived from Ulysses observations [*McComas et al.*, 2000]. Note that ΔU changes rapidly between about 10°–35°. This indicates an area of high turbulence activity where low and high speed streams are colliding and interacting. As such, we expect shear to be greater in this region than at the other, quieter, latitudes.

[81] The length Δr is the scale over which streams interact. This scale is not related to λ, which describes the approximate size of the energy-containing scales. There is some evidence for Δr increasing linearly with heliocentric density [*Whang*, 1991], but, to our knowledge, there are no large-scale observations to confirm this. Unfortunately, we also have no observations to constrain $r/\Delta r$.

[82] We note, however, that we can match observations against the model results to determine empirical values of C_{sh}. At higher latitudes (>35°), a value of 0.5 for C_{sh} produces results that match well against observations [*Breech et al.*, 2005]. Close to the ecliptic, values near unity for C_{sh} work well [*Matthaeus et al.*, 2004].

[83] With these considerations in mind, we adopt the following procedure for determining $r/\Delta r$ and setting C_{sh}. At higher latitudes, we choose $r/\Delta r$ to be a constant such that $C_{sh} \approx 0.5$. Lower than about 35°, we expect shear to increase due to the increase in ΔU. Gradients leading to the increased ΔU may be either "gentle" or "steep." Turbulence would only develop from steep gradients. We will assume about half the gradients in this latitude range are steep, leading to turbulence. We use the same constant for $r/\Delta r$ as at higher latitudes, but now multiply by 1/2 to account for the distribution of gradients. Finally, at lower latitudes, C_{sh} is set to unity and smoothly joined. This leads to the C_{sh} profile shown in the lower right panel of Figure 1. Note that this profile maintains a higher level of shear in the 15°–35° band.

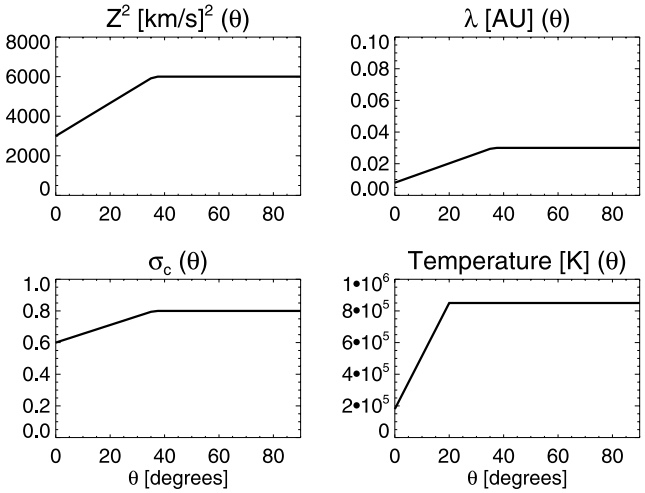

Figure 2. Boundary profiles of the various turbulence quantities at 0.3 AU as a function of latitude with respect to the solar ecliptic. The profile values were chosen to provide good agreement with observations. Note the break near 35°, which was deliberately patterned after a similar break seen in Ulysses observations for velocity and density [*McComas et al.*, 2000].

3.2. θ-Dependence of the Boundary Conditions

[84] The transport equations are coupled hyperbolic ODEs in the radial coordinate, and therefore solutions can be obtained at any angular position in the heliosphere by specifying the turbulence energy, cross helicity, correlation scale and temperature variables at an inner radius. The initial values for these quantities are allowed to vary latitudinally. It is assumed the solutions are independent of spherical azimuthal coordinate, that is, the modeled heliospheric plasma is axisymmetric. With the model, we can then compute the behavior of the turbulence quantities everywhere in the heliosphere beyond the inner boundary surface. Here the inner boundary is set at 0.3 AU and we employ observational data from several sources to guide our selection of boundary conditions as a function of latitude.

[85] For low latitudes, substantial guidance regarding mean values and variability of turbulence parameters is given by the Helios, Voyager, and Pioneer missions, as well as the Omni data set at 1 AU near earth, which includes IMP and ISEE data. Since we are interested in latitudinal structure, the Ulysses mission data set is especially valuable, and indeed, for high latitudes Ulysses mission data are our main source of observational constraints. We have focused attention on Ulysses high-latitude scans during or near solar minimum conditions [*McComas et al.*, 2000]. In most cases we need to extrapolate the observational data back to 0.3 AU from large radial distance ($\sim$2–5 AU). (Ulysses also provides further low-latitude profile data during its rapid equatorial passes.)

[86] Figure 2 shows typical boundary profiles employed for the turbulence quantities when integrating out from 0.3 AU. The profiles were created by choosing values in the ecliptic and at higher latitudes to give good agreement with observations. Ulysses observations [*McComas et al.*, 2000] show a clear break near 35°, which is replicated in our boundary profiles. The exception is the temperature profile where the break is observed earlier, near 20°. The break may be a result of weaker shear as the solar wind becomes a more pure fast wind.

[87] For the pickup protons, the relevant inner boundary is at 1 AU rather than 0.3 AU (see section 2.5). The two quantities to be prescribed there are the solar wind density and the Alfvén speed, V_A. The left panel of Figure 3 shows the density profile at 1 AU, taken from *McComas et al.* [2000]. The right panel shows the computed $V_A = B_0/\sqrt{4\pi\rho}$ at 1 AU. Here, B_0 is the magnitude of the background magnetic field modeled as the Parker spiral [*Parker*, 1958] and ρ is the density, taken from the boundary profile and scaled as $\rho \sim 1/r^2$.

[88] We remark that the boundary profiles shown in Figures 2 and 3 are not authoritative in the sense that they explain all observations. More likely, there is some probability distribution (frequency of occurrence) of initial values for the turbulence quantities. However, the near earth, 1 AU data sets are the only ones extensive enough to provide such probability distributions. (See, for instance, *Padhye et al.* [2001] for details of the distributions of mean magnetic field strengths and mean magnetic turbulence energy density at 1 AU, which were found to be approximately lognormally distributed.) The profiles shown are an attempt to approximate the most probable value of such distributions.

3.3. Selection of Other Parameters

[89] We specify other parameters as follows; We take $M = 1/2$, which is a typical 1 AU value consistent with the transverse cases discussed earlier with a constant winding angle of $\psi = 45°$; see equation (26). While this choice is more appropriate at 1 AU, the mixing effect is small compared to C_{sh} and a more accurate value makes little difference.

[90] We adopt a constant Alfvén ratio of $r_A = 1/2$, which corresponds to setting $\sigma_D = -1/3$. This value for r_A is observed frequently [*Roberts et al.*, 1987b], although some parcels of turbulence may have higher values [*Roberts et al.*, 1990].

3.4. Summary of Parameter Selection

[91] The transport model includes many parameters and boundary conditions. Some are fixed constants, while others may vary latitudinally but not radially and others may vary

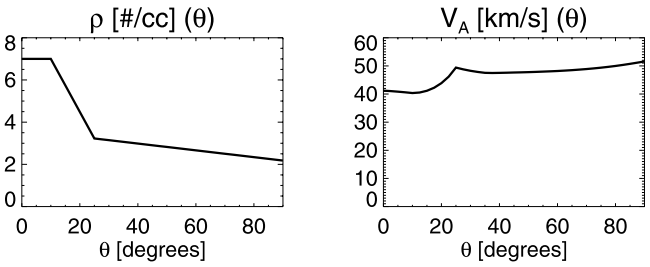

Figure 3. Prescribed latitudinal profiles at 1 AU for the density and Alfvén speed V_A. V_A is computed from a Parker spiral and the density profile, assuming the density scales as $\rho \sim 1/r^2$.

Table 1. Summary of the Various Parameters and Quantities That Appear in the Transport Model[a]

Symbol	Description	Value
α, β	Kármán–Taylor constants	$\alpha = 2$ $\beta = 0.8$
U	solar wind speed	radially constant, latitudinally varying, Figure 1
Csh	strength of shear driving	radially constant, latitudinally varying, Figure 1
M	underlying turbulence symmetry	constant, $M = 1/2$
σ_D	energy difference between **v**, **b** fields	constant, $\sigma_D = -1/3$
r_A	Alfvén ratio	constant, $r_A = 1/2$
ρ	proton number density	$\rho \sim 1/r^2$, Figure 3
$\ddot{E}_{PI}$	energy from pickup proton interaction	radially varying, equation (53), section 2.5
$L_{\rm cav}$	ionization cavity	$L_{\rm cav} = 8$ AU
V_A	Alfvén speed	varies according to the Parker spiral
n_h	hydrogen density at termination shock	constant, $n_h = 0.1$/cc
$\tau_{\rm ion}$	neutral ionization time at 1 AU	constant, $\tau_{\rm ion} = 10^6$ s
r	heliocentric distance (AU)	
Z^2	total turbulence energy	transported quantity, equation (2), Figure 2
λ	size energy containing scales	transported quantity, equation (3), Figure 2
σ_c	normalized cross helicity	transported quantity, equation (4), Figure 2
T	(proton) temperature	transported quantity, equation (5), Figure 2

[a]References to figures showing the boundary values for latitudinally varying quantities are given. Equation numbers are also given for those quantities that vary radially.

with both latitude and distance. Table 1 provides a summary of the different parameters and turbulence quantities.

4. Model Results

4.1. Calibration With Existing Spacecraft Data Sets

[92] Using the boundary profiles of the previous section, we can numerically solve equations (2)–(5) to obtain the turbulence transport. The equations were solved along radial spokes using IDL's fourth-order Runge–Kutta solver with a step size of 0.02 AU. Figures 4 and 5 show results in the ecliptic and at 75° latitude, respectively. The solid line in both figures is the solution computed using the boundary profiles from Figure 2. The other solutions shown have minor variations in the boundary values in order to encompass most of the observational data. The observational data comes from published data sets, with a few supplements from our own analyses. The ecliptic data use Voyager 2 and Helios data [*Roberts et al.*, 1987a; *Zank et al.*, 1996; *Smith et al.*, 2001]. The higher latitude data are from Ulysses [*Bavassano et al.*, 2000a, 2000b; *Breech et al.*, 2005].

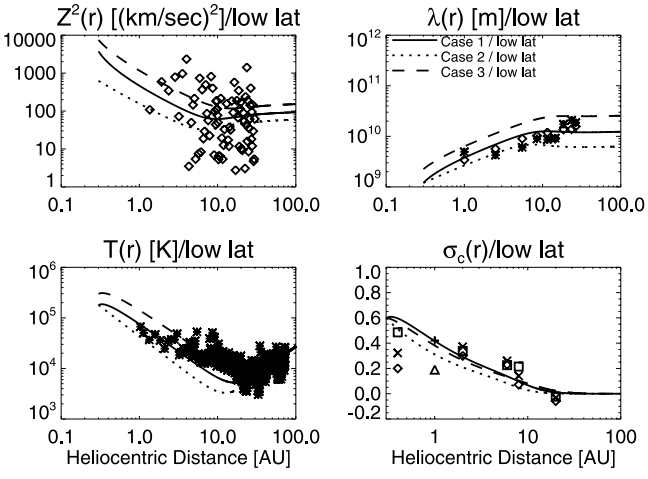

Figure 4. Solutions for the model taken in the ecliptic. Observational data are from Voyager 2, except for the inner heliosphere points for σ_c (which came from Helios and Omni). With the exception of the Omni σ_c point, the data have been used in previous studies [*Smith et al.*, 2001; *Zank et al.*, 1996; *Roberts et al.*, 1987a]. The solid line uses the typical boundary profiles shown in earlier Figures. The other solutions are minor variations to show that the model can encompass a variety of observations. The initial values for Case 1 are $Z_0^2 = 3000$ (km/s)^2, $\lambda_0 = 0.008$ AU, $\sigma_{c0} = 0.60$ and $T_0 = 1.8$ e5 K. For case 2, $Z_0^2 = 500$ (km/s)^2, $\lambda_0 = 0.008$ AU, $\sigma_{c0} = 0.60$ and $T_0 = 1.8$ e5 K. For case 3, $Z_0^2 = 6000$ (km/s)^2, $\lambda_0 = 0.015$ AU, $\sigma_{c0} = 0.60$ and $T_0 = 3$ e5 K.

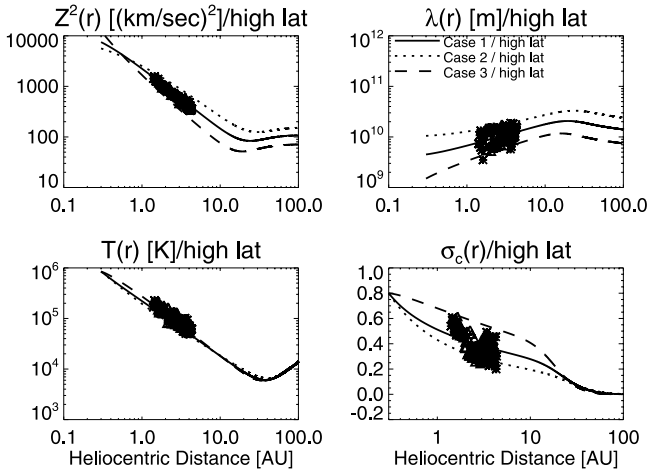

Figure 5. Solutions for the model taken at $\theta = 75°$. All observational data are from Ulysses [*Bavassano et al.*, 2000a, 2000b; *Breech et al.*, 2005]. The solid line uses the typical boundary profiles of section 3.2, while the other two solutions are minor variations. Inner boundary values for Case 1 are $Z_0^2 = 6000$ (km/s)^2, $\lambda_0 = 0.03$ AU, $\sigma_{c0} = 0.80$ and $T_0 = 8.5$ e5 K. For case 2, $Z_0^2 = 4500$ (km/s)^2, $\lambda_0 = 0.07$ AU, $\sigma_{c0} = 0.80$ and $T_0 = 8.5$ e5 K. For case 3, $Z_0^2 = 10{,}000$ (km/s)^2, $\lambda_0 = 0.01$ AU, $\sigma_{c0} = 0.80$ and $T_0 = 8.5$ e5 K.

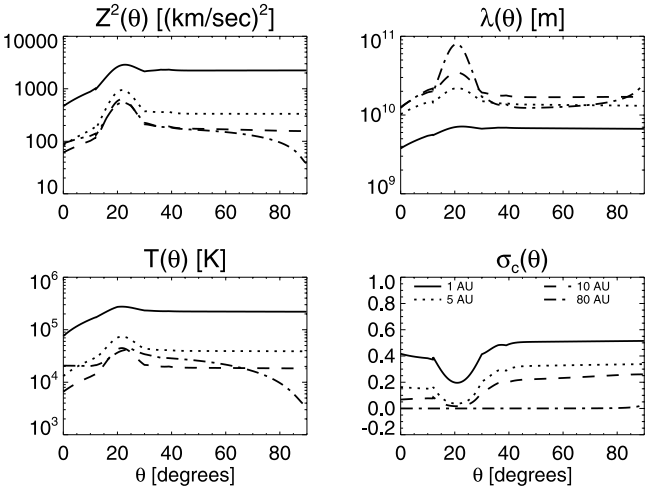

Figure 6. Solutions for the model taken at particular radial values. Each of the four turbulence quantities are shown as functions of latitude. There is a noticeable spike (depression in the case of σ_c) at the high shear layer (between about 15°–35°).

[93] The ecliptic observations show considerable variations in Z^2 and T. These variations may be due to "pollution" by high speed streams, solar cycle variations, or both. In contrast, the higher latitude Z^2 and T are much more tightly grouped. These differences are also reflected in the model results. The higher latitude solutions follow each other closely, while the solutions in the ecliptic are more spread out.

4.2. Computation of the Distribution of Turbulence Throughout the Heliosphere

[94] We can obtain further results by computing the solutions of equations (2)–(5) along radial spokes at varying latitudes. In particular, results were computed radially from 0.3 AU to 100 AU, with a step size of 0.2 AU, and 0° to 90° in latitude, with a step size of 0.14°.

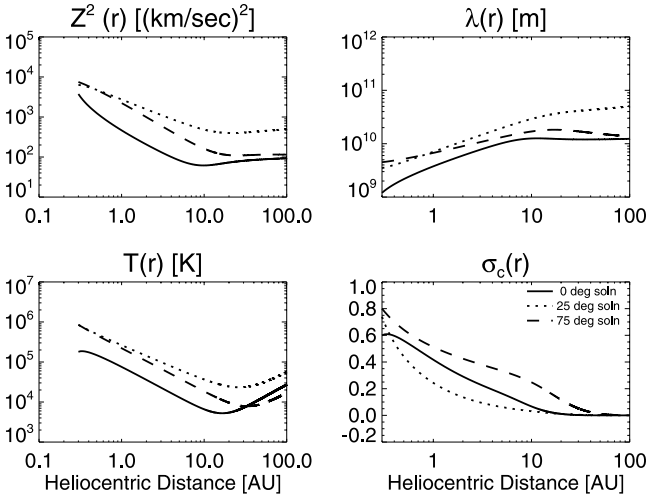

Figure 7. Solutions for the model taken at particular latitudes. The ecliptic plane and 75° solution are shown in Figures 4 and 5. The 25° solution shown here is in the high shear layer and shows higher levels of energy, higher temperature, longer correlation scales and suppressed levels of cross helicity.

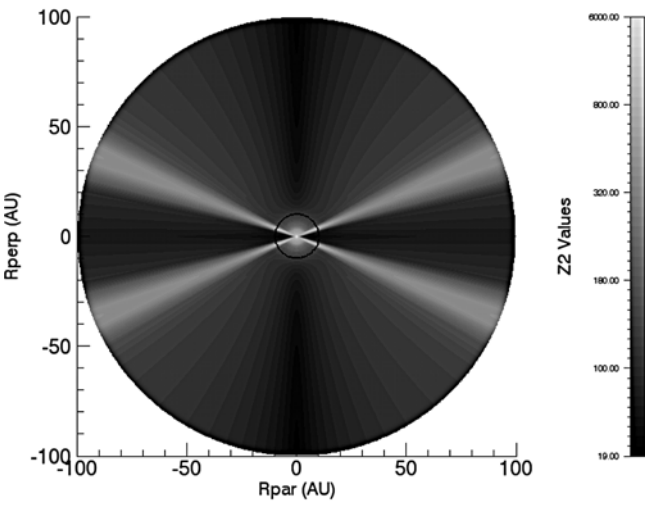

Figure 8. Z^2 distribution from 0 to 100 AU. The center circle is at r = 10 AU. The bands of higher energy occur at the layer of high shear.

[95] Figure 6 shows solutions for the transport model taken at particular radial values. In nearly all the solutions shown, there is a noticeable spike (depression in the case of σ_c) near the high shear layer. Figure 7 shows solutions for the model taken at different latitudes. Of particular interest is the 25° solution, which is in the high shear layer. This solutions shows elevated levels of energy and temperature, longer correlation lengths and suppressed cross helicity.

[96] A more complete view of the data can be obtained by computing shaded contour plots for each of the turbulence quantities. These results are shown in Figures 8–15, plotted as a function of Rpar, the coordinate lying in the ecliptic,

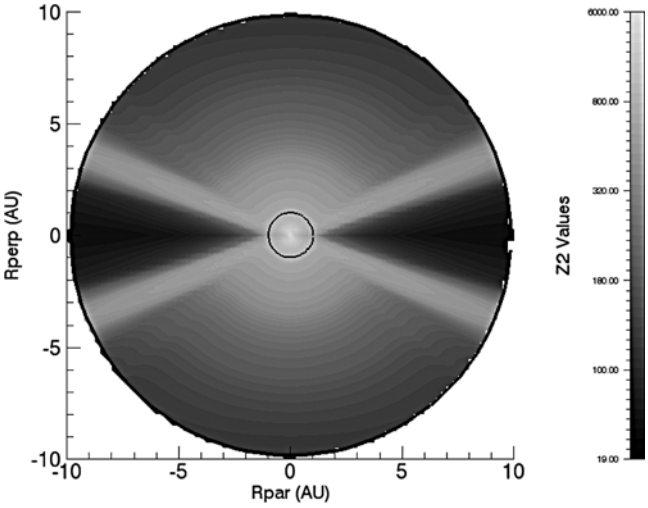

Figure 9. Z^2 distribution from 0 to 10 AU. The center circle is at r = 1 AU. Outside of the ecliptic, the inner heliosphere is more energetic than the outer parts.

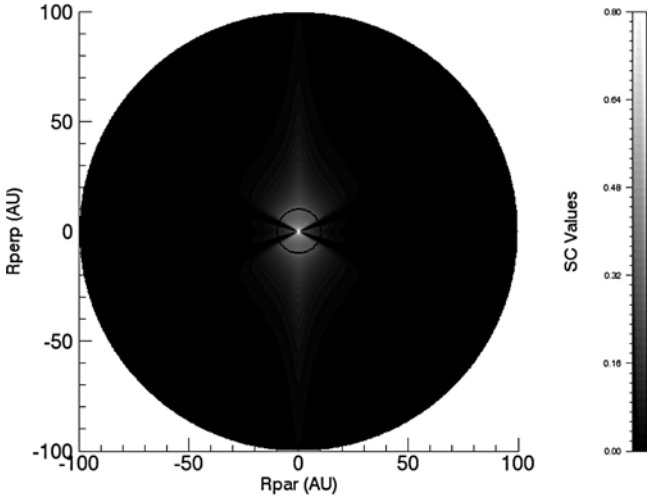

Figure 10. σ_c distribution from 0 to 100 AU. The center circle is at r = 10 AU. Shear and pickup proton interactions suppress the cross helicity by producing equal amounts of inward and outward fluctuations. Over the poles, where shear and pickup proton effects are lessened, higher Alfvénicity tends to linger.

and Rperp which is perpendicular to the ecliptic. Two sets of shaded contour plots are shown for each of the turbulence quantities; one from 0–100 AU and the other a zoom-in for 0–10 AU.

[97] The most striking feature is the "bands" at $\theta \approx \pm 35°$, present in all the distribution plots. These are layers of active turbulence, e.g., with higher energy, higher temperature, larger correlation scales, and depressed cross helicities compared to nearby latitudes. The bands are a result of stream shear, modeled by C_{sh}, and indeed setting $C_{sh} = 0$ removes the bands. They appear at the location of the high C_{sh} peak seen in Figure 1.

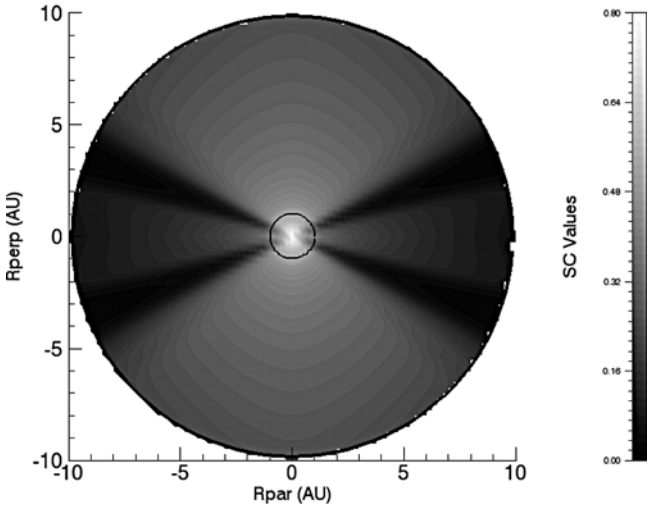

Figure 11. σ_c distribution from 0 to 10 AU. The center circle is r = 1 AU. Except at the shear layer, σ_c tends to decrease slowly.

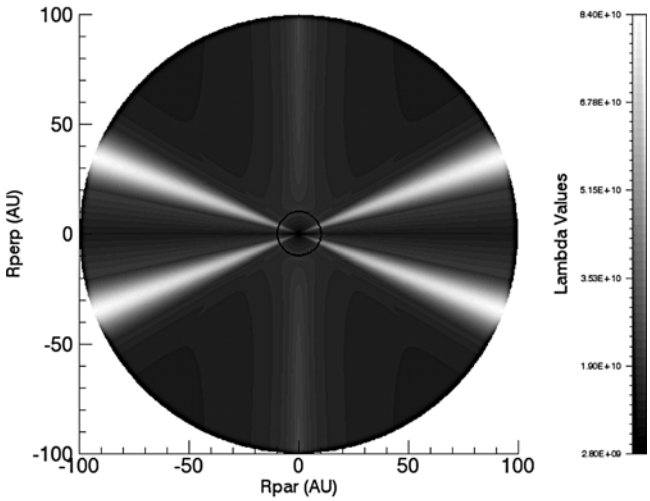

Figure 12. λ distribution from 0 to 100 AU. The center circle is at r = 10 AU.

[98] As seen from equation (2), the shear driving weakens with increasing heliocentric distance. Dissipation then acts to remove more energy from the turbulence, which would cause the bands to fade further out in the heliosphere. However, the pickup protons switch on near 8 AU creating another source of driving. The new driving deposits energy into the turbulence and maintains the higher levels of energy seen in the bands. This can also be seen in Figures 4, 5, and 7 where the shear layer solution decreases in energy, but still has more energy than the ecliptic or high latitude solutions. When the pickup protons turn on, energy is added to all of the solutions.

[99] Another feature in the profiles (see Figures 10 and 14) is that the pickup proton effects are suppressed over the poles. This arises because of the rapid decrease of the Alfvén speed over the poles in the Archimedean spiral

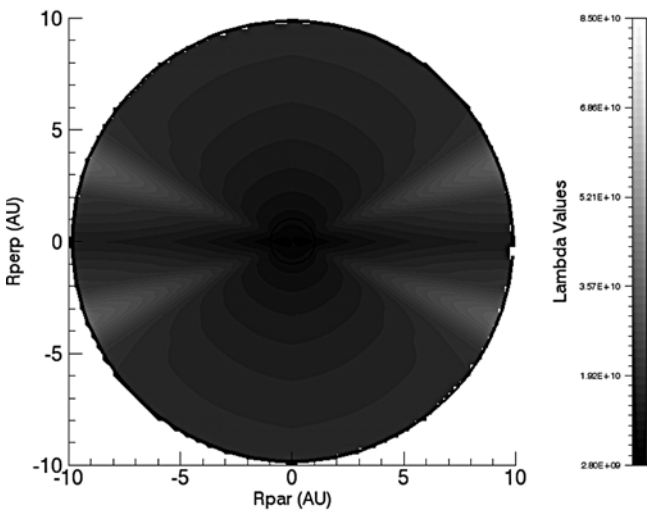

Figure 13. λ distribution from 0 to 10 AU. The center circle is at r = 1 AU. The λ values tend to be more depressed in the inner heliosphere than in the outer.

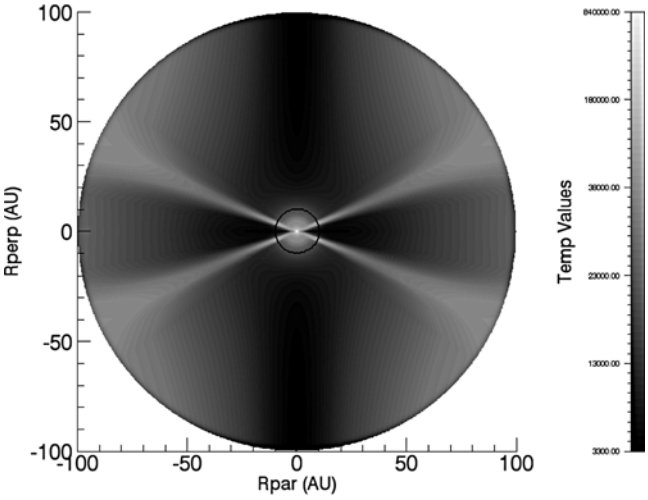

Figure 14. T distribution from 0 to 100 AU. The center circle is $r = 10$ AU. Because of the shear and pickup proton interactions, the shear layer and outer parts of the heliosphere tend to be warm. Over the poles, where these effects are lessened, the protons tend to be cooler.

magnetic field model, which suppresses the amount of energy available in the scattering process.

[100] The distribution of Alfvénicity, or preponderance of outwards traveling fluctuations is also evident (Figures 10–11). Alfvénicity is high in the inner heliosphere, but decreases toward the outer heliosphere due to expansion, shear, and pickup proton effects. There is substantial latitude variation. The poleward spikes show that Alfvénicity is maintained to higher distance at high latitudes due to the suppressed shear and pickup proton effects, but still eventually decreases. On the other hand, Alfvénicity decreases more rapidly near the heliospheric equator, where pickup proton effects are large. The most rapid decrease of Alfvénicity, as seen in Figure 11, occurs at intermediate latitudes, near the regions of strongest average shear driving.

[101] The turbulent energy distributions in Figures 8 and 9 also show that past a few AU, there is less energy in the ecliptic than in nearby latitudes. A similar effect is seen outside of the shear layer, but the effect is more pronounced in the ecliptic. We suggest this is due to more efficient dissipation. Past a few AU, effects of pickup protons and shear depress the Alfvénicity, which increases the efficiency of the dissipation through the f^+ term in equation (2). This, combined with the smaller similarity scale and wind speed, enables more rapid dissipation in the ecliptic than at other latitudes. The energy provided by shear and pickup proton driving is not enough to overcome the dissipation. At higher latitudes (excluding the poles), a similar process is occurring, but the dissipation is lessened due to larger similarity scale, faster wind speed, and lingering Alfvénicity.

[102] The similarity scale distributions in Figures 12 and 13 show somewhat less structure than the other quantities, particularly within 10 AU. However, they do show large values systematically near the region of large shear, and this persists to large heliocentric distances. Over the poles, the similarity scale shows a tendency to increase slightly beyond a few AU. This is due to the decreasing Alfvénicity and the weakness of pickup proton effects there. The increase in λ is only slight, since the turbulent energy available over the poles is small. In the high shear layers, however, λ increases to larger values due to the higher amounts of turbulent energy present.

[103] Figure 15 shows that, in the inner parts of the heliosphere, the protons tend to be warm. The exception to this is in the ecliptic past about 3 AU, where there does not appear to be much energy that can be dissipated and turned into heat. The effect does not last, however, as Figure 14 shows that the proton temperature begins to increases further out in the heliosphere. This is due to the pickup protons providing energy. Over the poles, the proton temperature rapidly decreases due to reduced shear and reduced strength of the pickup proton interactions.

[104] In summary, the model results show elevated levels of turbulence in the high shear layer. Turbulence is depressed over the poles due to lessened shear interaction and the lack of pickup proton interactions. Additionally, the inner heliosphere (0–10 AU) shows different structures than the outer heliosphere (>10 AU).

5. Conclusions

[105] We have presented the derivation and results of a four equation turbulence transport model for solar wind fluctuations. The transported quantities are turbulence energy Z^2, similarity scale λ, normalized cross helicity σ_c, and (proton) temperature, T. The model includes driving of the turbulence from stream shear interactions, mixing, and pickup proton effects. Parameters and values at the inner boundary were tuned to match known observations at both low and high latitudes. All parameters take on values that are physically reasonable, and that can be motivated either empirically or by simple analytical estimates. On the basis of the numerical results of the model, we would expect that

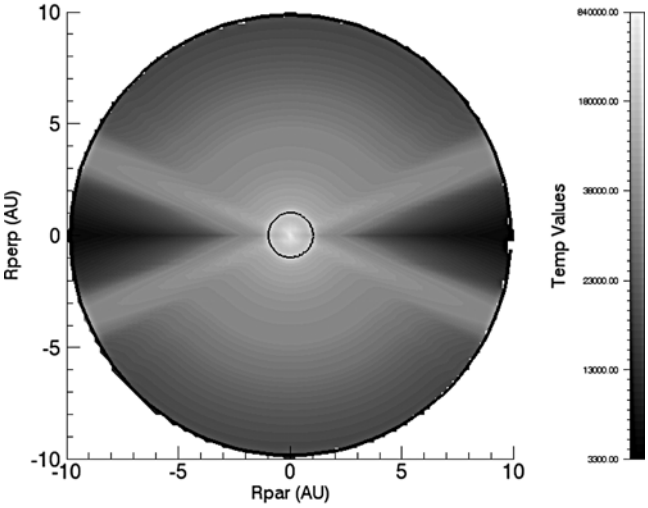

Figure 15. T distribution from 0 to 10 AU. The center circle is at $r = 1$ AU. Overall, the inner heliosphere tends to be much warmer than the outer heliosphere.

heliospheric turbulence would experience a layer of increased turbulence activity between about 15° and 35° latitude. Over the poles, turbulence is depressed due to the weak influence of both types of driving, namely via pickup protons and shear effects. Some of these results, such as the radial persistence of the features associated with the shear layer, may behave rather differently in the outer heliosphere when nonaxisymmetric effects, and three dimensional transport equations, are implemented. Even in their two-dimensional form, however, the present results are a step forward in understanding the physical basis for the distribution of turbulence through the heliosphere. Accordingly, these results can be useful in studying cosmic ray modulation and the heating of the solar wind.

[106] **Acknowledgments.** This research is supported in part by the Delaware Space Grant College and Fellowship Program (NASA grant NNG05GO92H), and by NASA grants NNG04GA54G, NNG06GD47G, NNX07AH73G, NNG04GB95G and NNX07AH75G, and NSF grants ATM-0539995 and ATM-0635863.

[107] Garry Zank thanks the reviewers for their assistance in evaluating this paper.

References

Batchelor, G. K. (1970), *The Theory of Homogeneous Turbulence*, CUP, University of Cambridge, Cambridge, UK.

Bavassano, B., M. Dobrowolny, G. Fanfoni, F. Mariani, and N. F. Ness (1982a), Statistical properties of fluctuations associated with high-speed streams from Helios-2 observations, *Sol. Phys.*, *78*, 373–384.

Bavassano, B., M. Dobrowolny, F. Mariani, and N. F. Ness (1982b), Radial evolution of power spectra of interplanetary turbulence, *J. Geophys. Res.*, *87*, 3617–3622.

Bavassano, B., E. Pietropaolo, and R. Bruno (2000a), Turbulence in the polar wind: A statistical study on cross helicity and residual energy variations, *J. Geophys. Res.*, *105*, 12,697–12,704.

Bavassano, B., E. Pietropaolo, and R. Bruno (2000b), On the evolution of outward and inward fluctuations in the polar wind, *J. Geophys. Res.*, *105*, 15,959–15,964.

Belcher, J. W., and L. Davis Jr. (1971), Large-amplitude waves in the interplanetary medium: 2, *J. Geophys. Res.*, *76*, 3534–3563.

Breech, B., W. H. Matthaeus, L. J. Milano, and C. W. Smith (2003), Probability distributions of the induced electric field of the solar wind, *J. Geophys. Res.*, *108*(A4), 1153, doi:10.1029/2002JA009529.

Breech, B., W. H. Matthaeus, J. Minnie, S. Oughton, S. Parhi, J. W. Bieber, and B. Bavassano (2005), Radial evolution of cross helicity in high-latitude solar wind, *Geophys. Res. Lett.*, *32*, L06103, doi:10.1029/2004GL022321.

Bruno, R., and V. Carbone (2005), The solar wind as a turbulence laboratory, *Living Rev. Solar Phys.*, *2*, (Available at: http://www.livingreviews.org/lrsp-2005-4).

Burlaga, L. (1974), Interplanetary stream interfaces, *J. Geophys. Res.*, *79*, 3717–3725.

Coleman, P. J. (1966), Hydromagnetic waves in the interplanetary plasma, *Phys. Rev. Lett.*, *17*, 207–211.

Coleman, P. J. (1968), Turbulence, viscosity, and dissipation in the solar wind plasma, *Astrophys. J.*, *153*, 371–388.

Dobrowolny, M., A. Mangeney, and P. Veltri (1980), Fully developed anisotropic hydromagnetic turbulence in interplanetary space, *Phys. Rev. Lett.*, *45*, 144–147.

Elsässer, W. M. (1950), The hydromagnetic equations, *Phys. Rev.*, *79*, 183.

Grappin, R., U. Frisch, J. Léorat, and A. Pouquet (1982), Alfvénic fluctuations as asymptotic states of turbulence, *Astron. Astrophys.*, *105*, 6–14.

Hossain, M., P. C. Gray, D. H. Pontius Jr., W. H. Matthaeus, and S. Oughton (1995), Phenomenology for the decay of energy-containing eddies in homogeneous turbulence, *Phys. Fluids*, *7*, 2886–2904.

Isenberg, P. A. (2005), Turbulence-driven solar wind heating and energization of pickup protons in the outer heliosphere, *Astrophys. J.*, *623*, 502–510.

Isenberg, P. A., C. W. Smith, and W. H. Matthaeus (2003), Turbulent heating of the distant solar wind by interstellar pickup protons, *Astrophys. J.*, *592*, 564–573.

Marsch, E., and C.-Y. Tu (1989), Dynamics of correlation functions with Elsässer variables for inhomogeneous turbulence, *J. Plasma Phys.*, *41*, 479–491.

Marsch, E., and C.-Y. Tu (1990a), On the radial evolution of turbulence in the inner heliosphere, *J. Geophys. Res.*, *95*, 8211–8229.

Marsch, E., and C.-Y. Tu (1990b), Spectral and spatial evolution of compressible turbulence in the inner solar wind, *J. Geophys. Res.*, *95*, 11,945–11,956.

Matthaeus, W. H., and M. L. Goldstein (1982), Measurement of the rugged invariants of magnetohydrodynamic turbulence in the solar wind, *J. Geophys. Res.*, *87*, 6011–6028.

Matthaeus, W. H., M. L. Goldstein, and D. C. Montgomery (1983), Turbulent generation of outward-traveling interplanetary fluctuations, *Phys. Rev. Lett.*, *51*, 1484–1487.

Matthaeus, W. H., M. L. Goldstein, and D. A. Roberts (1990), Evidence for the presence of quasi-two-dimensional nearly incompressible fluctuations in the solar wind, *J. Geophys. Res.*, *95*, 20,673–20,683.

Matthaeus, W. H., S. Oughton, D. Pontius, and Y. Zhou (1994a), Evolution of energy containing turbulent eddies in the solar wind, *J. Geophys. Res.*, *99*, 19,267–19,287.

Matthaeus, W. H., Y. Zhou, G. P. Zank, and S. Oughton (1994b), Transport theory and the WKB approximation for interplanetary fluctuations, *J. Geophys. Res.*, *99*, 23,421–23,430.

Matthaeus, W. H., G. P. Zank, and S. Oughton (1996), Phenomenology of hydromagnetic turbulence in a uniformly expanding medium, *J. Plasma Phys.*, *56*, 659–675.

Matthaeus, W. H., G. P. Zank, C. W. Smith, and S. Oughton (1999), Turbulence, spatial transport, and heating of the solar wind, *Phys. Rev. Lett.*, *82*, 3444–3447.

Matthaeus, W. H., J. Minnie, B. Breech, S. Parhi, J. W. Bieber, and S. Oughton (2004), Transport of cross helicity and the radial evolution of Alfvénicity in the solar wind, *Geophys. Res. Lett.*, *31*, L12803, doi:10.1029/2004GL019645.

Matthaeus, W. H., S. Dasso, J. M. Weygand, L. J. Milano, C. W. Smith, and M. G. Kivelson (2005), Spatial correlation of solar-wind turbulence from two-point measurements, *Phys. Rev. Lett.*, *95*, 231101, doi:10.1103/PhysRevLett.95.231101.

McComas, D. J., et al. (2000), Solar wind observations over Ulysses' first full polar orbit, *J. Geophys. Res.*, *105*, 10,419–10,434.

Neugebauer, M., B. E. Goldstein, D. J. McComas, S. T. Suess, and A. Balogh (1995), Ulysses observations of microstreams in the solar wind from coronal holes, *J. Geophys. Res.*, *100*, 23,389–23,395.

Oughton, S., and W. H. Matthaeus (1995), Linear transport of solar wind fluctuations, *J. Geophys. Res.*, *100*, 14,783–14,799.

Oughton, S., K.-H. Rädler, and W. H. Matthaeus (1997), General second-rank correlation tensors for homogeneous magnetohydrodynamic turbulence, *Phys. Rev. E*, *56*, 2875–2888.

Oughton, S. (2003), Solar wind fluctuations: Waves and turbulence, in *Solar Wind Ten*, vol. 679, edited by M. Velli, R. Bruno, and F. Malara, pp. 421–426, AIP, Melville, N.Y., doi:10.1063/1.1618626.

Padhye, N., C. W. Smith, and W. H. Matthaeus (2001), Distribution of magnetic field components in the solar wind plasma, *J. Geophys. Res.*, *106*, 18,635–18,650.

Parker, E. N. (1958), Dynamics of the interplanetary gas and magnetic fields, *Astrophys. J.*, *128*, 664–676.

Pouquet, A., M. Meneguzzi, and U. Frisch (1986), Growth of correlations in magnetohydrodynamic turbulence, *Phys. Rev. A*, *33*, 4266–4275.

Roberts, D. A., M. L. Goldstein, L. W. Klein, and W. H. Matthaeus (1987a), Origin and evolution of fluctuations in the solar wind: Helios observations and Helios-Voyager comparisons, *J. Geophys. Res.*, *92*, 12,023–12,035.

Roberts, D. A., L. W. Klein, M. L. Goldstein, and W. H. Matthaeus (1987b), The nature and evolution of magnetohydrodynamic fluctuations in the solar wind: Voyager observations, *J. Geophys. Res.*, *92*, 11,021–11,040.

Roberts, D. A., M. L. Goldstein, and L. W. Klein (1990), The amplitudes of interplanetary fluctuations: Stream structure, heliocentric distance, and frequency dependence, *J. Geophys. Res.*, *95*, 4203–4216.

Roberts, D. A., M. L. Goldstein, W. H. Matthaeus, and S. Ghosh (1992), Velocity shear generation of solar wind turbulence, *J. Geophys. Res.*, *97*, 17,115–17,130.

Smith, E., and J. Wolfe (1976), Observations of interaction regions and corotating shocks between one and five au: Pioneer 10 and 11, *Geophys. Res. Lett.*, *3*, 137–140.

Smith, C. W., W. H. Matthaeus, G. P. Zank, N. F. Ness, S. Oughton, and J. D. Richardson (2001), Heating of the low-latitude solar wind by dissipation of turbulent magnetic fluctuations, *J. Geophys. Res.*, *106*, 8253–8272.

Smith, C. W., P. A. Isenberg, W. H. Matthaeus, and J. D. Richardson (2006), Turbulent heating of the solar wind by newborn interstellar pickup protons, *Astrophys. J.*, *638*, 508–517.

Tennekes, H., and J. L. Lumley (1972), *A First Course in Turbulence*, MIT Press, Cambridge, Mass.

Townsend, A. A. (1976), *The Structure of Turbulent Shear Flow*, CUP, Cambridge, Mass.

Tu, C.-Y., and E. Marsch (1993), A model of solar wind fluctuations with two components: Alfvén waves and convective structures, *J. Geophys. Res.*, *98*, 1257–1276.

von Kármán, T., and L. Howarth (1938), On the statistical theory of isotropic turbulence, *Proc. R. Soc., Ser. A*, *164*, 192–215.

Whang, Y. C. (1991), Shock interactions in the outer heliosphere, *Space Sci. Rev.*, *57*, 339–388.

Williams, L. L., G. P. Zank, and W. H. Matthaeus (1995), Dissipation of pickup-induced waves: A solar wind temperature increase in the outer heliosphere?, *J. Geophys. Res.*, *100*, 17,059–17,067.

Zank, G. P., W. H. Matthaeus, and C. W. Smith (1996), Evolution of turbulent magnetic fluctuation power with heliospheric distance, *J. Geophys. Res.*, *101*, 17,093–17,107.

Zhou, Y., and W. H. Matthaeus (1990a), Transport and turbulence modeling of solar wind fluctuations, *J. Geophys. Res.*, *95*, 10,291–10,311.

Zhou, Y., and W. H. Matthaeus (1990b), Remarks on transport theories of interplanetary fluctuations, *J. Geophys. Res.*, *95*, 14,863–14,871.

J. W. Bieber, B. Breech, W. H. Matthaeus, and J. Minnie, Department of Physics and Astronomy and Bartol Research Institute, University of Delaware, Newark, DE 19716, USA. (breech@cis.udel.edu)

P. A. Isenberg and C. W. Smith, Institute for the Study of Earth, Oceans and Space, and Department of Physics, University of New Hampshire, Durham, NH 03284, USA.

S. Oughton, Department of Mathematics, University of Waikato, Private Bag 3105, Hamilton 3240, New Zealand.